PCCP

Accepted Manuscript

ROYAL SOCIETY OF CHEMISTRY

www.rsc.org/pccp

Journal Name

ARTICLE

Synthesis, Structure and Dehydrogenation Mechanism of Calcium Amidoborane Hydrazinates

Received 00th January 20xx,
Accepted 00th January 20xx

DOI: 10.1039/x0xx00000x

www.rsc.org/

Zhao Li[a,b], Teng He*[a], Guotao Wu[a], Weidong Chen[a,b], Yong Shen Chua[d], Jianping Guo[b], Dong Xie[a], Xiaohua Ju[a], Ping Chen*[a,c]

The calcium amidoborane hydrazinates, $Ca(NH_2BH_3)_2{\cdot}nN_2H_4$, were firstly synthesized by reacting different molar ratios of $Ca(NH_2BH_3)_2$ and N_2H_4. In particular, $Ca(NH_2BH_3)_2$ and N_2H_4 with molar ratio of 1:2 crystallizes into orthorhombic symmetry $P2_12_12_1$ space group with the lattice parameters of a = 6.6239(4) Å, b = 13.7932(6) Å, c = 4.7909(2) Å. The dehydrogenations of calcium amidoborane hydrazinates are two-step reactions, exhibiting superior dehydrogenation properties compared with that of pristine $Ca(NH_2BH_3)_2$. For $Ca(NH_2BH_3)_2{\cdot}1/2N_2H_4$, approximately 4.6 equiv. hydrogen (or 7.9 wt% hydrogen) can be released at 150 °C. Kinetic analysis shows that the activation energies for the two steps of hydrogen desorption from $Ca(NH_2BH_3)_2{\cdot}2N_2H_4$ are much lower than those of pristine $Ca(NH_2BH_3)_2$, suggesting improvement in the dehydrogenation kinetics of $Ca(NH_2BH_3)_2$ after coordinating with N_2H_4. Isotopic labeling results show that the driving force for the dehydrogenation of calcium amidoborane hydrazinates is the combination of protonic hydrogen and hydridic hydrogen ($H^{\delta+}$ and $H^{\delta-}$). In addition, the initial H_2 releasing from calcium amidoborane hydrazinates originates from the interaction of [-BH_3] and N_2H_4, rather than [-BH_3] and [-NH_2] (in [-NH_2BH_3]).

1. Introduction

Due to the increasingly serious global energy crisis, searching and utilizing efficient alternative energy sources are inevitable, among which hydrogen can be viewed as a clean and promising energy carrier.[1-3] However, lack of efficient hydrogen storage material on board is one of the most difficult challenges for the coming "hydrogen economy". In the past decade, much efforts have been given to ammonia borane (AB, NH_3BH_3), which has a high hydrogen capacity (*ca*. 19.6 wt%) and moderate dehydrogenation properties.[4-6] However, its drawbacks such as severe dehydrogenation kinetic barrier, emission of poisonous by-products and sample foaming limit its direct application.[7, 8] To solve the problems, one of the most important options is to replace H in [-NH_3] group from AB with metals forming metal amidoborane (MAB), which is implemented by reacting AB with metal hydrides including LiH[9], NaH[9], KH[10], CaH_2[11, 12], MgH_2[13], SrH_2[14]. Besides MABs derived from AB-hydride interactions, metal amidoborane ammoniates can be obtained through the interactions between amides[15], imides or nitrides[16] with AB. Alternatively, a straight-forward method, which is the absorption of stoichiometric NH_3 by metal amidoboranes, can also give rise to metal amidoborane ammoniates. The ligand of NH_3 in metal amidoborane ammoniates not only improves the hydrogen capacity, but also moderates the dehydrogenation kinetics. For instance, although $Ca(NH_2BH_3)_2{\cdot}2NH_3$ desorbs NH_3 in open system forming $Ca(NH_2BH_3)_2$, it releases H_2 directly in close system at 150°C.[17, 18] Other metal amidoborane ammoniates, such as $LiNH_2BH_3{\cdot}NH_3$, can reversibly desorb/adsorb NH_3 at room temperature. However, the decomposition of $LiNH_2BH_3{\cdot}NH_3$ can produce 3.0 equiv. H_2 under ammonia at low temperature.[19] The examples above have revealed that the cation properties including electronegativity, charge and ionic radius may significantly affect its coordination capability to a ligand, which will alter the activity of the ligand and further lead to different dehydrogenation performance.[20] For example, Li^+ and Mg^{2+} have similar ionic radius but Mg bears more positive charges and thus executes stronger coordination with NH_3. As a result, $Mg(NH_2BH_3)_2{\cdot}NH_3$ releases H_2 rather than NH_3 under dynamic Ar flow different from those of $LiNH_2BH_3{\cdot}NH_3$.[21] In addition, coordination strength is affected by the number of ligands attaching to the metal center as well. $Mg(NH_2BH_3)_2{\cdot}3NH_3$ releases NH_3 and H_2 under dynamic flow, whereas $Mg(NH_2BH_3)_2{\cdot}NH_3$ prefers to give off only H_2 under the same conditions.[22] In general, the ligand, like ammonia, plays a vital role not only in stabilizing amidoboranes and increasing the hydrogen capacity, but also in altering the dehydrogenation behavior. Therefore, it is of great interest to explore other ligands with high hydrogen content and optimize the dehydrogenation properties of metal amidoboranes.

Recently, hydrazine (N_2H_2) has attracted much attention in hydrogen production. Hydrazine hydrate can release hydrogen at

[a] Dalian National Laboratory for Clean Energy, Dalian Institute of Chemical Physics, Chinese Academy of Sciences, 457, Zhongshan Road, Dalian, 116023, China.
[b] University of the Chinese Academy of Sciences, Beijing 100049, China.
[c] State Key Laboratory of Catalysis, Dalian Institute of Chemical Physics, Chinese Academy of Sciences, 457, Zhongshan Road, Dalian, 116023, China.
[d] School of Chemical Sciences, Universiti Sains Malaysia, 11800, Pulau Pinang, Malaysia.

Electronic Supplementary Information (ESI) available: [XRD, IR and ^{11}B solid state MAS NMR of the prepared samples, MS analyses of the gaseous products and TPD files]. See DOI: 10.1039/x0xx00000x

room temperature with the presence of catalysts.[23, 24] Since there is lone pair electrons on N, hydrazine can coordinate with [-BH_3] forming hydrazine borane ($N_2H_4BH_3$) which show improved dehydrogenation properties after being modified by metal hydrides (NaH, LiH and KH *etc.*).[25-27] Additionally, hydrazine can be used as the reductants to regenerate spent fuels of AB and lithium amidoborane to their original state in ammonia solution, achieving a complete hydrogen cycle.[28, 29] Considering the combination of protonic $H^{\delta+}$ and hydridic $H^{\delta-}$ to form hydrogen, hydrazine with $H^{\delta+}$ can coordinate with $H^{\delta-}$ containing compounds and modify their dehydrogenation properties. Recently, several borohydride hydrazinates were synthesized and they have been demonstrated the improved dehydrogenation kinetics with different dehydrogenation route.[30, 31] Similarly, hydrazinate of lithium amidoborane ($LiNH_2BH_3{\cdot}NH_2NH_2$) has also been synthesized. Although it exhibited an improved dehydrogenation properties as compared with pristine $LiNH_2BH_3$,[32] the underlying dehydrogenation mechanism was not well understood. Since interaction of cations and ligands can obviously affect the properties, more efforts should be spent to synthesize other amidoborane hydrazinates, which alter the hydrogen storage performances. In the present study, we have successfully prepared calcium amidoborane hydrazinates ($Ca(NH_2BH_3)_2{\cdot}nN_2H_4$), with $Ca(NH_2BH_3)_2{\cdot}2N_2H_4$ exhibited a new compound crystallizes in an orthorhombic cell with the space group of $P2_12_12$ and the lattice parameters of a = 6.6239(4) Å, b = 13.7932(6) Å, c = 4.7909(2) Å. Improved dehydrogenation properties was reported as compared with pristine $Ca(NH_2BH_3)_2$. More importantly, isotope-labelling method was employed to investigate its dehydrogenation mechanism.

2. Experimental section

2.1 Sample preparation

Ca powders (99%, Alfa Aesar), $(NH_4)_2CO_3$ (99%, Acros), $NaBH_4$(98%, Aldrich), $NaBD_4$(98%, Aldrich) and D_2O(99%, Aldrich) were used without further purification. NH_3BH_3 was homemade by the metathesis of $(NH_4)_2CO_3$ and $NaBH_4$through ball-milling according to R1. $NaBH_4$ and pre-ball milled $(NH_4)_2CO_3$ were dissolved into tetrahydrofuran (THF) with a 2:1 molar ratio and ball-milled for 4h at 40°C. Then the filtrate was concentrated under vacuum to obtain AB.[33] NH_3BD_3 was prepared by the same procedure but with $NaBD_4$ instead of $NaBH_4$. ND_3BH_3 was synthesized by repeating dissolution of AB in D_2O and evaporation under vacuum at room temperature three times.[34] $Ca(NH_2)_2$ was prepared by the reaction of Ca powder and liquid NH_3 (R2). $Ca(NH_2BH_3)_2$ was made by dissolving the mixture of NH_3BH_3 and $Ca(NH_2)_2$ in THF according to R3. The solvent was then removed via rotor evaporation under reduced pressure, yielding powdery $Ca(NH_2BH_3)_2$. Similarly, $Ca(NH_2BD_3)_2$ were synthesized via the same methods but with NH_3BD_3 instead of NH_3BH_3. $Ca(ND_2BH_3)_2$ were synthesized by using the deuterium complexes like ND_3BH_3 and $Ca(ND_2)_2$ according to R4.

$$(NH_4)_2CO_3 + 2NaBH_4 \rightarrow 2NH_3BH_3 + Na_2CO_3 + 2H_2 \quad \text{R1}$$

$$\mathrm{Ca} + 2NH_3 \rightarrow Ca(NH_2)_2 + H_2 \quad \text{R2}$$

$$\mathrm{Ca}(NH_2)_2 + 2NH_3BH_3 \rightarrow Ca(NH_2BH_3)_2 + 2NH_3 \quad \text{R3}$$

$$\mathrm{Ca}(ND_2)_2 + 2ND_3BH_3 \rightarrow Ca(ND_2BH_3)_2 + 2ND_3 \quad \text{R4}$$

All experiments were performed under strictly anaerobic and anhydrous conditions in the MBRAUN glovebox filled with purified argon. To synthesize calcium amidoborane hydrazinate samples with ratios of 1/0.5, 1/1, 1/2, 1/3, around 300 mg $Ca(NH_2BH_3)_2$and calculated hydrazine were placed separately into a sealed bottle at room temperature. Due to the vapour pressure, hydrazine can automatically absorb into $Ca(NH_2BH_3)_2$ overnight. The samples were then ball milled on a Retsch PM 400 planetary mill at 150 rpm under an inert atmosphere for 2 h.

2.2 Dehydrogenation and characterizations

To examine the new structures and the mechanism of hydrogen evolution from the $Ca(NH_2BH_3)_2{\cdot}nN_2H_4$ system, the samples before and after dehydrogenation were characterized by Fourier transform infrared (FTIR), X-ray diffraction (XRD), solid-state ^{11}B magic angle spinning nuclear magnetic resonance (MAS NMR). FTIR spectra were recorded by a Varian 3100 FTIR spectrometer at room temperature. XRD data were collected on a PANalytical X'pert diffractometer equipped with Cu Kα radiation (40kV and 40mA). NMR experiments were implemented at room temperature on a Bruke AVANCE 500 MHz NMR spectrometer (11.7 T). All of those solid samples were spun at 10 kHz with 4 mm ZrO_2 rotor in diameter, in which the powders were fully loaded. In homemade temperature programmed desorption(TPD) system combined with mass spectrometer (MS, Hiden HPR-20) measurements, a dynamic flow mode was applied, in which purified argon was used as carrier gas and the heating rate was set at 2°C/min. Volumetric release experiments were performed on a homemade Sieverts-type apparatus to quantify the hydrogen evolution. 50~60 mg sample was heated to a given temperature at a ramping rate of 2 °C/min.

2.3 First-principles calculations method:

First-principles calculations were performed using the Vienna *ab initio* simulation package (VASP), which is based on DFT and the pseudopotential plane wave method. [35, 36] The projector augmented wave (PAW) potentials were used with a cut-off energy of 500 eV.[37] The generalized gradient approximation (GGA) due to Perdew and Wang (GGA-PW91) was used to treat the electronic exchange-correlation energy.[38] According to their lattice constants, different k-points meshes generated by the Monkhorst-Pack method were selected. In geometry optimizations, experimental atomic positions and cell parameters were used as starting models for the relaxations. Full ionic and volumetric relaxations were carried out until the self-consistency was achieved within a tolerance of the total energy of 0.01 meV and atomic forces of 0.01 eV/Å.

3. Results and discussions

3.1 Syntheses and structures

The as-prepared calcium amidoborane hydrazinates were examined by XRD as shown in Fig. S1. As the amount of hydrazine absorbed on $Ca(NH_2BH_3)_2$ increases, the phase of $Ca(NH_2BH_3)_2$ disappears gradually, accompanying with the appearance of new phases. From

FTIR in Fig. S2, $Ca(NH_2BH_3)_2$-nN_2H_4 (n = 1/2, 1, 2) samples exhibit different spectra to that of $Ca(NH_2BH_3)_2$. The B-H stretching bands ranging from 2150 to 2270 cm^{-1} in $Ca(NH_2BH_3)_2$-nN_2H_4 show a red shift compared with that of $Ca(NH_2BH_3)_2$, indicating the weakened B-H bonds. However, the N-H vibration bands of $Ca(NH_2BH_3)_2 \cdot nN_2H_4$ split into several peaks due to the complicated coordination environments. From ^{11}B MAS NMR results in Fig. S3, the chemical shift at -17.9 ppm that belongs to sp^3 hybridized [-BH_3] in $Ca(NH_2BH_3)_2$ shifts to -24.3 ppm as the increasing of hydrazine gradually, indicating the change of B environment and the formation of new species. The high field shift to -24.3 ppm of $Ca(NH_2BH_3)_2 \cdot nN_2H_4$ indicates a higher electron density surrounds B compared with pristine $Ca(NH_2BH_3)_2$,[17] which may be attributed to the electron donation of N_2H_4 when it coordinates with $Ca(NH_2BH_3)_2$ and results in elongated B-H bonds.

To explore and solve the crystal structures of calcium amidoborane hydrazinates, the XRD pattern and the Rietveld fits of newly synthesized $Ca(NH_2BH_3)_2 \cdot 2N_2H_4$ are shown in Fig. 1. The crystal structure is then partially solved by using direct space methods under this space group. Due to the uncertainty of H positions, first-principles molecular dynamics simulated annealing are then performed to confirm the $Ca(NH_2BH_3)_2$ and NH_2NH_2 configuration with the lowest energy. Rietveld structural refinement on the optimal structural candidate is performed using the GSAS package on the XRD data. The $Ca(NH_2BH_3)_2$ and NH_2NH_2 are kept as rigid bodies with common refined bond lengths and bond angles constrained as reasonable values due to the inadequate number of observations. One $Ca(NH_2BH_3)_2$ and one NH_2NH_2 group together with lattice parameters are refined, yielding the agreement factors of Rwp = 5.95%, Rp = 4.45%.

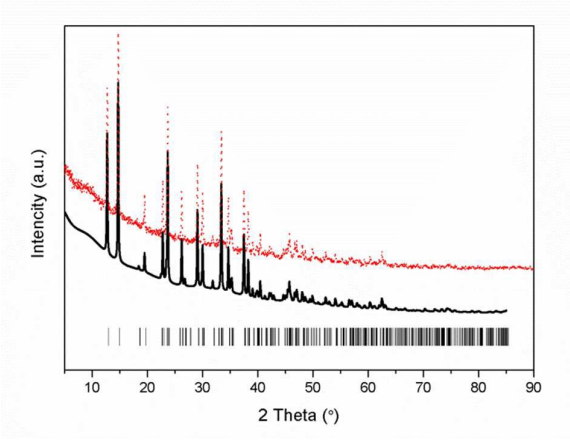

Fig.1 Experimental (dots), fitted (line) of XRD profiles for $Ca(NH_2BH_3)_2 \cdot 2N_2H_4$ at 298 K (Cu Kα radiation). Vertical bars indicate the calculated positions of Bragg peaks of $Ca(NH_2BH_3)_2 \cdot 2N_2H_4$.

The new sets of diffraction peaks emerging in $Ca(NH_2BH_3)_2 \cdot 2N_2H_4$ can be well indexed by an orthorhombic $P2_12_12$ space group with a = 6.6239(4) Å, b = 13.7932(6) Å, c = 4.7909(2) Å. The crystal structure of $Ca(NH_2BH_3)_2 \cdot 2N_2H_4$ and local coordination of Ca^{2+} cation are shown in Fig. 2. And the interatomic distances in $Ca(NH_2BH_3)_2 \cdot 2N_2H_4$ as compared with pristine $Ca(NH_2BH_3)_2$ and pristine hydrazine can be found in Table 1. Each Ca^{2+} coordinates with two $[NH_2BH_3]^-$ groups and four NH_2NH_2 groups, leading to distorted octahedral environment, which is preferred in the commonly observed Ca (VI) complex hydrides, *e.g.*, $Ca(NH_2)_2$[39] , CaNH[40], and $Ca(BH_4)_2$[41].

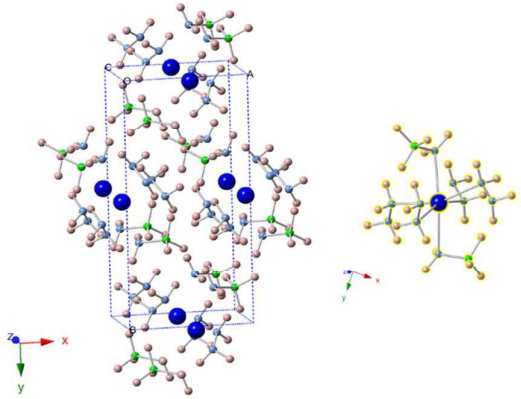

Fig.2 (left) Crystal structure of $Ca(NH_2BH_3)_2 \cdot 2N_2H_4$. Calcium is represented by blue spheres, boron by green spheres, nitrogen by purple spheres, hydrogen by pink spheres.(right) Coordination environment of Ca^{2+}. Each Ca^{2+} coordinates with four N_2H_4 groups and two [$BH_2NH_3^-$] groups.

The distances between Ca^{2+} and N in the adjacent NH_2NH_2 are 2.563 and 2.579 Å, similar to the Ca-N distances in coordinate bond, such as $Ca(BH_4)_2 \cdot 2N_2H_4$ (2.540 Å)[31]. At the same time, the Ca^{2+} directly bonds with two $NH_2BH_3^-$ ions giving the closest Ca-N distance of 2.486 Å, similar to Ca-N distances in ionic bonds, such as $Ca(NH_2BH_3)_2 \cdot 2NH_3$ (2.521Å)[17] and $Ca(NH_2)_2$ (2.411-2.573 Å)[39]. Since the coordination of NH_2NH_2 to $Ca(NH_2BH_3)_2$ is through the donation of a lone pair electrons, Ca^{2+} will bear higher electron density than that in pristine $Ca(NH_2BH_3)_2$, resulting in the elongated Ca-N distance (Ca-[NH_2BH_3]) in $Ca(NH_2BH_3)_2 \cdot 2N_2H_4$ as shown in Table 1. Similarly, due to the lower electron density of N, N-H (in NH_2NH_2 ligand) distances in $Ca(NH_2BH_3)_2 \cdot 2N_2H_4$ are longer than that of the pristine hydrazine, indicating the activation of N-H bond in hydrazinate. Furthermore, each N atoms in one hydrazine molecule is coordinated by a Ca^{2+} from opposite direction, which may lead to the elongated distance between N-N. Moreover, the B-H and N-H bond distances in amidoborane anion, $NH_2BH_3^-$ have lengthened, agreeing with FTIR and NMR results. From the crystal structure, it was found that the $H^{\delta+}$ (in NH_2NH_2 or NH_2BH_3) has a short distance with its neighbouring $H^{\delta-}$ in [-BH_3], ranging from 2.00~2.37 Å (less than 2.4 Å), which indicates the establishment of dihydrogen bonding network. Such interaction of the oppositely charged $H^{\delta+}$ (in NH_2NH_2 and NH_2) and $H^{\delta-}$ (in BH_3^-) may consequently contribute to the elongated N-H and B-H bonds in $Ca(NH_2BH_3)_2 \cdot 2N_2H_4$. It is reported that the dihydrogen bonding network in ammonia borane is primarily responsible for the stability of the molecular crystal at room temperature.[5] The dihydrogen bonding network and the ionic/electrostatic interactions between Ca and NH_2BH_3/N_2H_4 ligands in $Ca(NH_2BH_3)_2 \cdot 2N_2H_4$ are thus responsible for the structural stabilization and are likely to have positive impacts on their dehydrogenation. Although $Ca(NH_2BH_3)_2$-$3N_2H_4$ also shows new diffraction peaks in XRD pattern, the structure was not resolved due to poor crystallinity.

Table 1 Interatomic distances (Å) in $Ca(NH_2BH_3)_2 \cdot 2N_2H_4$ compared with pristine $Ca(NH_2BH_3)_2$ and hydrazine at room temperature.

•	$Ca(NH_2BH_3)_2 \cdot 2N_2H_4$	$Ca(NH_2BH_3)_2$	NH_2NH_2
Ca-N bonds(Å)	2.486(Ca-[NH_2BH_3]) 2.563~2.579 (Ca- [NH_2NH_2])	2.466	-
N-H bonds(Å)	1.022([NH_2BH_3]) 1.025~1.030(NH_2NH_2)	1.020	1.021
B-N bonds(Å)	1.558	1.546	-
B-H bonds(Å)	1.242~1.246	1.230~1.250	-
N-N bonds(Å)	1.452	-	1.449

3.2 Dehydrogenation of $Ca(NH_2BH_3)_2 \cdot nN_2H_4$(n=1/2, 1, 2)

TPD-MS measurement is employed to investigate the dehydrogenation properties of $Ca(NH_2BH_3)_2 \cdot nN_2H_4$ compared with the pristine $Ca(NH_2BH_3)_2$. As shown in Fig. 3, pristine $Ca(NH_2BH_3)_2$ releases hydrogen with a broad peak centered at around 150 °C identical to that in literature.[17] Obviously, the decomposition of $Ca(NH_2BH_3)_2 \cdot nN_2H_4$ (n = 1/2, 1, 2) can be viewed as a two-step process: the first dehydrogenation process occurs in the temperature range of 100~125°C and the second is between 160~185°C. It is known that the number of ligands coordinating with the metal center contributes to the different decomposition behaviours. Similarly, the more ligands coordinate with a metal center, the easier they would be detached.[20] However, a different phenomenon is observed in the case of $Ca(NH_2BH_3)_2 \cdot nN_2H_4$. The signal of ligand N_2H_4 is undetectable during TPD-MS experiments, indicating that the coordinated N_2H_4 prefers to react with $Ca(NH_2BH_3)_2$ instead of self-detachment. For $Ca(NH_2BH_3)_2 \cdot 2N_2H_4$ sample mentioned above (Fig. 3d), it starts to release hydrogen at around 98 °C with a peak centered at 118°C, accompanying with evolution of NH_3 in the first step. The evolution of NH_3 should be attributed to the excess of N from N_2H_4 in the system which results in the side reaction (*i.e.*, deammonization) that occurs simultaneously with dehydrogenation. Therefore, in order to suppress the ammonia evolution, the content of hydrazine is reduced to 1:1 ($Ca(NH_2BH_3)_2$:N_2H_4) (Fig. 3c). It can be found that the first dehydrogenation peak of $Ca(NH_2BH_3)_2$-N_2H_4 centered at 113°C is still companied with trace mount of ammonia. Further decreasing the amount of N_2H_4 to 0.5 resulted in no NH_3 release(Fig. 3b). This is likely due to the complete conversion of H^+ in N_2H_4 to H_2 when equal amount of $H^{\delta+}$ and $H^{\delta-}$ coexists in the sample. It was reported that the decomposition of hydrazine follows two competitive routes (R5 and R6) giving rise to H_2 and N_2 or N_2 and NH_3 under mild conditions even with the presence of noble or noble metal-like catalysts.[23, 24] However, no N_2 can be observed during the dehydrogenation/decomposition of $Ca(NH_2BH_3)_2 \cdot nN_2H_4$. Therefore, the evolution of NH_3 during the decomposition of $Ca(NH_2BH_3)_2 \cdot nN_2H_4$ (n=1/2, 1, 2) are not from the self-decomposition of hydrazine, which means the hydrogen is derived from the interaction of $Ca(NH_2BH_3)_2$ and hydrazine.

$$NH_2NH_2 \rightarrow N_2 + 2H_2 \quad \text{R5}$$

$$3NH_2NH_2 \rightarrow N_2 + 4NH_3 \quad \text{R6}$$

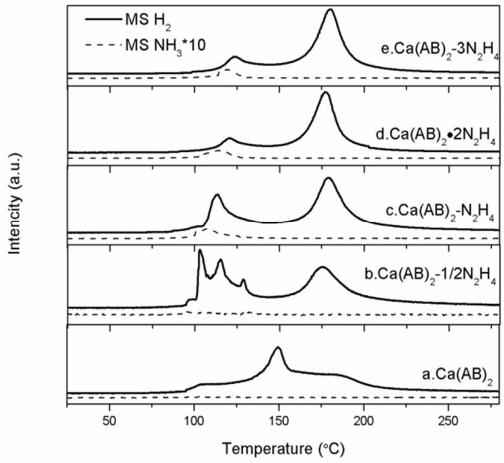

Fig.3TPD-MS results of $Ca(NH_2BH_3)_2$-nN_2H_4 complexes. The solid lines represent the signal of H_2 and the dotted lines represent the signal of NH_3.

Quantitative measurements on hydrogen desorption from the samples were subsequently investigated using a Sievert-type apparatus. It is known that the thermal decomposition pathway of $LiBH_4 \cdot NH_3$ can be altered by "locking" NH_3 in the vicinity of $LiBH_4$ to increase the chance of dehydrogenation rather than deammonization.[42] Similar approach was adopted to retain NH_3 in this study. As shown in Fig. 4, the pristine $Ca(NH_2BH_3)_2$ releases 2.6 equiv. H_2 (5.2 wt%) at 150 °C, identical to the literature.[17] Under the same condition, $Ca(NH_2BH_3)_2 \cdot 2N_2H_4$ can release more than 5.8 equiv. gas, which is composed of hydrogen and ammonia as detected by MS (Fig. S4). Approximately 4.6 equiv. of H_2 was evolved from both $Ca(NH_2BH_3)_2$-1/2N_2H_4 and $Ca(NH_2BH_3)_2$-N_2H_4 at 150°C within 12 hours, equivalent to 7.9 wt% and 7.0 wt% of hydrogen, respectively. Interestingly, no NH_3 was detected in the gaseous product (Fig. S4). Obviously, under the same condition, more H_2 can be released from $Ca(NH_2BH_3)_2$-nN_2H_4 than that from $Ca(NH_2BH_3)_2$,which indicates that the addition of N_2H_4 enhanced the dehydrogenation properties of $Ca(NH_2BH_3)_2$. Overall, $Ca(NH_2BH_3)_2$-1/2N_2H_4 with equal amount of $H^{\delta+}$ and $H^{\delta-}$produced more hydrogen (7.9 wt%) than other samples, which is worth of further investigation.

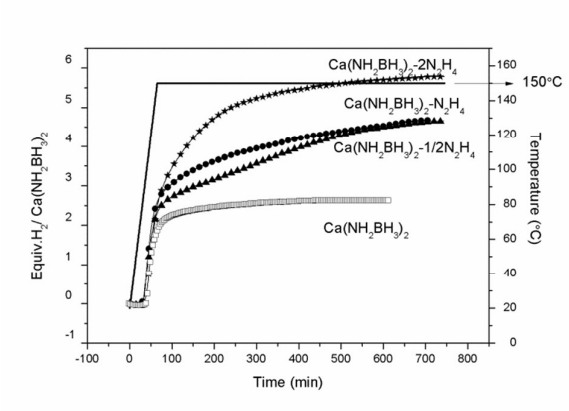

Fig. 4 Volumetric release measurements of (a) $Ca(NH_2BH_3)_2$, (b) $Ca(NH_2BH_3)_2$-$1/2N_2H_4$, (c) $Ca(NH_2BH_3)_2$-N_2H_4, (d) $Ca(NH_2BH_3)_2 \cdot 2N_2H_4$ at 150°C.

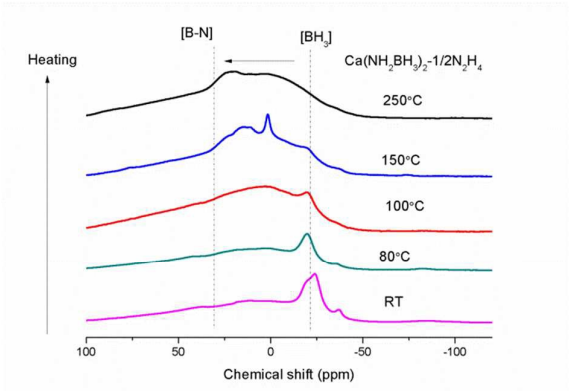

Fig. 5 ^{11}B MAS NMR spectra of $Ca(NH_2BH_3)_2$-$1/2N_2H_4$ and $Ca(NH_2BH_3)_2$-$1/2N_2H_4$ dehydrogenated at different temperatures.

In order to gain insight into the reaction process, the dehydrogenated products of $Ca(NH_2BH_3)_2$-$1/2N_2H_4$ at different dehydrogenation temperatures, *i.e.*, 80°C, 100°C, 150 °C, 250°C were collected to be characterized by XRD, FTIR and NMR. Due to the amorphous nature of the intermediates, no structural information can be obtained by XRD. As shown in the FTIR characterizations (Fig. S5) the B-H and N-H vibrations in the range of 3150 cm^{-1} to 3400 cm^{-1} and at 2200 cm^{-1} are weakened and broadened, respectively, as dehydrogenation progressing. A new vibration centered at 1600 cm^{-1}, which can be assigned to the [N=B=N] bond (Fig. S5),[43] gradually emerges upon increasing the temperatures. Agreeing with decreasing intensity of N-H and B-H vibrations, the relative intensity of sp^3 hybridized BH_3 resonance (-30 to -20 ppm) also decreases as dehydrogenation progressed. On the other hand, the resonances at ~3 ppm and 20~30ppm, which can be assigned to sp^2-hybridized B species (*i.e.*, N_2BH and BN_3) become more obvious. This result suggests that B-N bond was formed concomitantly with the release of H_2. Therefore, it is clear that B–N formation and the strong combination potential of the oppositely charged hydrogen atoms are the driving forces for the dehydrogenation process.

3.3 The kinetics of dehydrogenation

As mentioned above, the addition of N_2H_4 to $Ca(NH_2BH_3)_2$ enhanced the dehydrogenation kinetics as compared with pristine $Ca(NH_2BH_3)_2$. Therefore, the Kissinger method [Eq.1] was employed to determine the energy barrier in hydrogen desorption from $Ca(NH_2BH_3)_2$ and $Ca(NH_2BH_3)_2 \cdot 2N_2H_4$.

$$ln\left(\frac{\beta}{T_p^2}\right) = -\frac{Ea}{RT_p} + ln\left(\frac{AR}{E_a}\right) \qquad \text{Eq.1}$$

According to Eq.1, T_p is the peak temperature at which the maximum reaction rate is, β is the heating rate, E_a is the activation energy, A is the pre-exponential factor, and R is the gas constant. The maximum reaction-rate temperatures at different heating rates were collected by means of TPD measurements. The TPD profiles of hydrogen desorption from the $Ca(NH_2BH_3)_2 \cdot 2N_2H_4$ and $Ca(NH_2BH_3)_2$ samples at different ramping rates are shown in Fig. S6 and S7. It is observed that the peak temperatures shift monotonically to higher values when the ramping rate is increased from 2 to 8 K·min^{-1}. The dependence of $ln(E_a/T_p^2)$ to $1/T_p$ is linear (Fig. 6). The slopes of the fitted lines are used to determine the values of E_a. The results of E_a in the first and second dehydrogenation step for $Ca(NH_2BH_3)_2 \cdot 2N_2H_4$ and $Ca(NH_2BH_3)_2$ are shown in Table 2. The activation energies E_a for hydrogen desorption from $Ca(NH_2BH_3)_2 \cdot 2N_2H_4$ are around 98±5 kJ/mol in the first step and 102±4 kJ/mol in the second step, respectively. Both of them are lower than those of $Ca(NH_2BH_3)_2$, *ca.* 110±5 kJ/mol and 139±6 kJ/mol, suggesting the enhancement in dehydrogenation kinetics of $Ca(NH_2BH_3)_2$ when coordinates with N_2H_4.

Table 2 Values of E_a (the first and second step) determined by Kissinger plots.

Sample	E_a(kJ/mol) 1st Step	E_a(kJ/mol) 2nd Step
$Ca(NH_2BH_3)_2$	110±5	139±6
$Ca(NH_2BH_3)_2 \cdot 2N_2H_4$	98±5	102±4

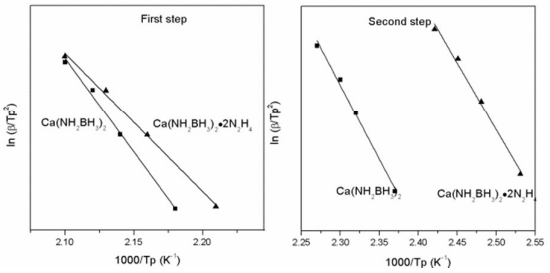

Fig. 6 The Kissinger's plots, which give the activation energy of hydrogen release from the $Ca(NH_2BH_3)_2$ and $Ca(NH_2BH_3)_2 \cdot 2N_2H_4$ samples.

3.4 The dehydrogenation mechanism

As mentioned in the section 3.2, the decomposition of hydrazine follows two competitive ways (R5 and R6). In this study, however, no nitrogen was released during the decomposition of $Ca(NH_2BH_3)_2{\cdot}nN_2H_4$, indicating that hydrogen release is not from the self-decomposition of hydrazine. Furthermore, the onset dehydrogenation temperature of $Ca(NH_2BH_3)_2{\cdot}nN_2H_4$ is lower than that of pristine $Ca(NH_2BH_3)_2$, which confirms that the hydrogen is released via the interaction of $Ca(NH_2BH_3)_2$ and N_2H_4. Considering that the dissociation energy of N–N bond is lower than that of N–H bond in hydrazine, the ''homogeneous dissociation'' of N–N bond forming $[{\cdot}NH_2]$ radicals may occur.[44] The produced $[{\cdot}NH_2]$ then reacts with $Ca(NH_2BH_3)_2$ to release H_2. In our previous work on $LiNH_2BH_3$-nN_2H_4, two possible dehydrogenation reaction mechanism were proposed, *i.e.* $LiN_2H_3BH_3$ intermediate pathway and combination of protonic hydrogen and hydridic hydrogen ($H^{\delta+}$ and $H^{\delta-}$) pathway. [32] More specifically, a $[{\cdot}NH_2]$ from "homogeneous dissociation" of N_2H_4 may attack the $[\text{-}NH_2]$ group or the $[\text{-}BH_3]$ group in $Ca(NH_2BH_3)_2$ alternatively to evolve H_2. However, it is still unable to figure out which group is attacked at the first step. Herein, to confirm the dehydrogenation mechanism, deuterium labeling experiments were conducted. Since three kinds of hydrogen atoms exist in $Ca(NH_2BH_3)_2$-$1/2N_2H_4$, *i.e.,* $H^{\delta+}$ in $[\text{-}NH_2BH_3]$, $H^{\delta+}$ in N_2H_4, and $H^{\delta-}$ in $[\text{-}NH_2BH_3]$, two deuterium substituted complexes $Ca(NH_2BD_3)_2{\cdot}1/2N_2H_4$ and $Ca(ND_2BH_3)_2{\cdot}1/2N_2H_4$ were synthesized and characterized by FTIR and XRD (Fig. S8 and S9) .

From the TPD-MS of $Ca(ND_2BH_3)_2{\cdot}1/2N_2H_4$ shown in Fig. 7a, although the desorbed gas is a mixture of H_2, HD and D_2, H_2 is the main gaseous product in the first stage. As mentioned above, the formation of H_2 should not derive from self-decomposition of hydrazine, therefore, the combination of $H^{\delta+}$ and $H^{\delta-}$ mechanism in the amidoborane hydrazinate should have taken place. Due to the fact that $H^{\delta+}$ on $Ca(ND_2BH_3)_2{\cdot}1/2N_2H_4$ should only come from N_2H_4 ligand, the strong H_2 signal as compared with HD and D_2 (Fig. 7a and inset) suggests that the first step dehydrogenation should be a result of the combination of $H^{\delta+}$ on N_2H_4 and $H^{\delta-}$ on BH_3 of $Ca(ND_2BH_3)_2$. Moreover, the appearance of HD and D_2 may be arising from the exchange of H-D at elevated temperature.[20] Additionally, the onset temperature of H_2 evolution from $Ca(ND_2BH_3)_2$-$1/2N_2H_4$ occurs at 74 °C, which is prior to those of HD and D_2 (Fig. 7a inserted), further confirming the $H^{\delta+}$ (NH_2NH_2) and $H^{\delta-}$ (BH_3) combination mechanism.

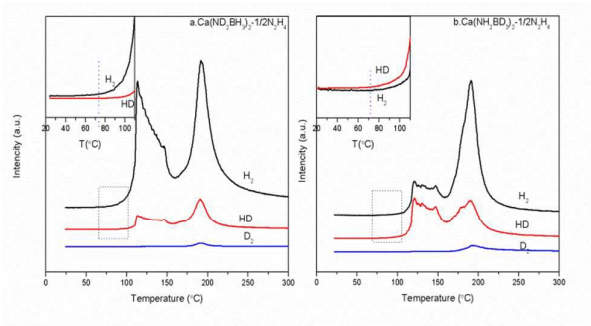

Fig.7 TPD-MS curves of $Ca(ND_2BH_3)_2{\cdot}1/2N_2H_4$ and $Ca(NH_2BD_3)_2{\cdot}1/2N_2H_4$.

In addition, the onset temperature of HD evolution from $Ca(NH_2BD_3)_2{\cdot}1/2N_2H_4$ advances 15 °C compared to that of H_2, which matches well with the phenomenon of $Ca(ND_2BH_3)_2{\cdot}1/2N_2H_4$ and provides the another proof for the protonic hydrogen-hydridic hydrogen($H^{\delta+}$ and $H^{\delta-}$) combination mechanism (Fig. 7b). As reported in the literature, "metal assisted hydride transfer " path via transferring a hydridic hydrogen atom from $[\text{-}BH_3]$ to get close to $[\text{-}NH_2]$ happened in the first-step dehydrogenation of $LiNH_2BH_3$ on the basis of gas-phase simulations.[45, 46] A bridged H could form through the hydride transfer in the form of Li···H···B,[45, 47, 48] which may be an active H in the transition state. This bridged H may also exist in the other metal amidoboanes and their derivatives during heat treatment, for example, $LiNH_2BH_3{\cdot}NH_3BH_3$ and $Ca(NH_2BH_3)_2{\cdot}2NH_3$. Therefore, during the thermal decomposition of these compounds, the combination of a $H^{\delta-}$(B) atom from metal amidoborane part and a $H^{\delta+}$(N) atom from the adjacent molecule (NH_3BH_3 or NH_3) could be observed.[18, 49] This may also happen in $Ca(NH_2BH_3)_2{\cdot}nN_2H_4$ material, which is confirmed by our isotopic labelling experiment. Therefore, we propose that the process of dehydrogenation goes through the following steps: 1. The "homogeneous dissociation" of N_2H_4 to form the $[{\cdot}NH_2]$ species; 2. The $[{\cdot}NH_2]$ attacks $[\text{-}BH_3]$ in $Ca(NH_2BH_3)_2$ with releasing H_2 by the ways of protonic hydrogen-hydridic hydrogen ($H^{\delta+}$ and $H^{\delta-}$) combination, excluding the metal hydrazine borane intermediate pathway[27, 50]. During the dehydrogenation, the H-D exchange will inevitably happen leading to complicated gaseous products. Therefore, we tentatively believe that the protonic hydrogen-hydridic hydrogen ($H^{\delta+}$ and $H^{\delta-}$) interaction is the main driving force in the whole dehydrogenation process.

The regeneration of the dehydrogenated products is also a vital important aspect for hydrogen storage materials. However, the dehydrogenation of NH_3BH_3 and its derivatives are usually exothermic, indicating the irreversibility of those compounds. Recently, it was reported that NH_3BH_3 or lithium amidoborane can be regenerated by using hydrazine in NH_3 solution[28, 29, 51]. Our recent result on the regeneration of lithium amidoborane hydrazinate by employing the same method also realized the partial regeneration of BH_3 species, indicating the feasibility of this method for hydrazinate.[32] Therefore, it is of great interest to apply the hydrazine reduction method to regenerate calcium amidoborane hydrazinates in the following investigation.

4. Conclusions

The calcium amidoborane hydrazinates with superior dehydrogenation properties were successfully synthesized, among which $Ca(NH_2BH_3)_2{\cdot}2N_2H_4$ crystallizes into orthorhombic symmetry $P2_12_12_1$ space group with the lattice parmeters of a = 6.6239(4) Å, b = 13.7932(6) Å, c = 4.7909(2) Å. Isotopic labelling experiment revealed that the protonic hydrogen from NH_2NH_2 would attack hydridic hydrogen from $[\text{-}BH_3]$ to form H_2 through the combination of $H^{\delta+}$ and $H^{\delta-}$ at the initial stage of the dehydrogenation for $Ca(NH_2BH_3)_2{\cdot}nN_2H_4$. However, more work is still needed in the fu-

ture to develop more materials with superior dehydrogenation properties and explore the dehydrogenation mechanism.

Acknowledgements

The authors would like to acknowledge financial support from the project of National Natural Science Funds for Distinguished Young Scholar (51225206), projects of National Natural Science Foundation of China (Grant Nos. U1232120, 51301161, 21473181 and 51472237) and project from Youth Innovation Promotion Association CAS, and Shanghai Synchrotron Radiation Facility (SSRF BL14B1) for providing the beam time.

References

1. N. Armaroli and V. Balzani, in *Energy for a Sustainable World*, Wiley-VCH Verlag GmbH & Co. KGaA, Weinheim, 2011, pp. I-XXI.
2. N. Armaroli and V. Balzani, *Angew. Chem. Int. Ed.*, 2007, **46**, 52-66.
3. N. Cao, J. Su, X. Hong, W. Luo and G. Cheng, *Chem.-Asian J.*, 2014, **9**, 562-571.
4. F. H. Stephens, V. Pons and R. T. Baker, *Dalton Trans.*, 2007, 2613-2626.
5. A. Staubitz, A. P. M. Robertson and I. Manners, *Chem. Rev.*, 2010, **110**, 4079-4124.
6. T. B. Marder, *Angew. Chem. Int. Ed.*, 2007, **46**, 8116-8118.
7. A. Gutowska, L. Y. Li, Y. S. Shin, C. M. M. Wang, X. H. S. Li, J. C. Linehan, R. S. Smith, B. D. Kay, B. Schmid, W. Shaw, M. Gutowski and T. Autrey, *Angew. Chem. Int. Ed.*, 2005, **44**, 3578-3582.
8. F. Baitalow, J. Baumann, G. Wolf, K. Jaenicke-Rossler and G. Leitner, *Thermochim. Acta*, 2002, **391**, 159-168.
9. Z. Xiong, C. K. Yong, G. Wu, P. Chen, W. Shaw, A. Karkamkar, T. Autrey, M. O. Jones, S. R. Johnson, P. P. Edwards and W. I. F. David, *Nat. Mater.* , 2008, **7**, 138-141.
10. H. V. K. Diyabalanage, T. Nakagawa, R. P. Shrestha, T. A. Semelsberger, B. L. Davis, B. L. Scott, A. K. Burrell, W. I. F. David, K. R. Ryan, M. O. Jones and P. P. Edwards, *J. Am. Chem. Soc.*, 2010, **132**, 11836-11837.
11. H. Wu, W. Zhou and T. Yildirim, *J. Am. Chem. Soc.*, 2008, **130**, 14834-14839.
12. A. E. Carre-Burritt, B. L. Davis, B. D. Rekken, N. Mack and T. A. Semelsberger, *Energy Environ. Sci.*, 2014, **7**, 1653-1656.
13. S.-K. Kim, S.-A. Hong, H.-J. Son, W.-S. Han, C. W. Yoon, S. W. Nam and S. O. Kang, *J. Mater. Chem. A*, 2014, **2**, 20243-20251.
14. H. Li, Q. Yang, X. Chen and S. G. Shore, *J. Organomet. Chem.* , 2014, **751**, 60-66.
15. K. R. Graham, T. Kemmitt and M. E. Bowden, *Energy Environ. Sci.*, 2009, **2**, 706-710.
16. Z. Xiong, Y. Chua, G. Wu, L. Wang, M. W. Wong, Z. M. Kam, T. Autrey, T. Kemmitt and P. Chen, *Dalton Trans.*, 2010, **39**, 720-722.
17. Y. S. Chua, G. Wu, Z. Xiong, T. He and P. Chen, *Chem. Mat.*, 2009, **21**, 4899-4904.
18. Y. S. Chua, W. Li, W. J. Shaw, G. Wu, T. Autrey, Z. Xiong, M. W. Wong and P. Chen, *ChemsusChem*, 2012, **5**, 927-931.
19. G. Xia, X. Yu, Y. Guo, Z. Wu, C. Yang, H. Liu and S. Dou, *Chem.-Eur. J.*, 2010, **16**, 3763-3769.
20. T. He, H. Wu, J. Chen, W. Zhou, G. Wu, Z. Xiong, T. Zhang and P. Chen, *Phys. Chem. Chem. Phys.* , 2013, **15**, 10487-10493.
21. Y. S. Chua, H. Wu, W. Zhou, T. J. Udovic, G. Wu, Z. Xiong, M. W. Wong and P. Chen, *Inorg. Chem.* , 2012, **51**, 1599-1603.
22. Y. S. Chua, G. Wu, Z. Xiong, A. Karkamkar, J. Guo, M. Jian, M. W. Wong, T. Autrey and P. Chen, *Chem. Commun.*, 2010, **46**, 5752-5754.
23. L. He, Y. Huang, A. Wang, X. Wang, X. Chen, J. J. Delgado and T. Zhang, *Angew. Chem. Int. Ed.*, 2012, **51**, 6191-6194.
24. S. K. Singh and Q. Xu, *J. Am. Chem. Soc.*, 2009, **131**, 18032-18033.
25. Y. S. Chua, Q. Pei, X. Ju, W. Zhou, T. J. Udovic, G. Wu, Z. Xiong, P. Chen and H. Wu, *J. Phys. Chem. C*, 2014, **118**, 11244-11251.
26. R. Moury, U. B. Demirci, T. Ichikawa, Y. Filinchuk, R. Chiriac, A. van der Lee and P. Miele, *ChemSusChem*, 2013, **6**, 667-673.
27. H. Wu, W. Zhou, F. E. Pinkerton, T. J. Udovic, T. Yildirim and J. J. Rush, *Energy Environ. Sci.*, 2012, **5**, 7531-7535.
28. A. D. Sutton, A. K. Burrell, D. A. Dixon, E. B. Garner, III, J. C. Gordon, T. Nakagawa, K. C. Ott, P. Robinson and M. Vasiliu, *Science*, 2011, **331**, 1426-1429.
29. Z. Tang, Y. Tan, X. Chen and X. Yu, *Chem. Commun.* , 2012, **48**, 9296-9298.
30. T. He, H. Wu, G. Wu, J. Wang, W. Zhou, Z. Xiong, J. Chen, T. Zhang and P. Chen, *Energy Environ. Sci.* , 2012, **5**, 5686-5689.
31. L. Zhang, S. Li, Y. Tan, Z. Tang, Z. Guo and X. Yu, *J. Mater. Chem. A*, 2014, **2**, 10682-10687.
32. T. He, H. Wu, G. Wu, Z. Li, W. Zhou, X. Ju, D. Xie and P. Chen, *J. Mater. Chem. A*, 2015, **3**, 10100-10106.
33. P. V. Ramachandran and P. D. Gagare, *Inorg. Chem.*, 2007, **46**, 7810-7817.
34. R. Cantelli, A. Paolone, O. Palumbo, F. Leardini, T. Autrey, A. Karkamkar and A. T. Luedtke, *J. Alloys Compd.* , 2013, **580**, S63-S66.
35. G. Kresse and J. Hafner, *Phys. Rev. B*, 1993, **47**, 558-561.
36. G. Kresse and J. Furthmüller, *Comput. Mater. Sci.* , 1996, **6**, 15-50.
37. G. Kresse and D. Joubert, *Phys. Rev. B*, 1999, **59**, 1758-1775.
38. J. P. Perdew and Y. Wang, *Phys. Rev. B*, 1992, **45**, 13244-13249.
39. J. Senker, H. Jacobs, M. Müller, W. Press, P. Müller, H. M. Mayer and R. M. Ibberson, *J. Phys. Chem. B* 1998, **102**, 931-940.
40. T. Sichla and H. Jacobs, *Z. Anorg. Allg. Chem.* , 1996, **622**, 2079-2082.

41. K. Miwa, M. Aoki, T. Noritake, N. Ohba, Y. Nakamori, S.-i. Towata, A. Züttel and S.-i. Orimo, *Phys. Rev. B*, 2006, **74**, 155122.
42. X. Zheng, G. Wu, W. Li, Z. Xiong, T. He, J. Guo, H. Chen and P. Chen, *Energy Environ. Sci.* , 2011, **4**, 3593-3600.
43. S. A. Kulinich, A. N. Zhukov, L. G. Sevast'yanova and K. P. Burdina, *Diamond Relat. Mater.* , 1999, **8**, 2152-2158.
44. J. P. Contour and G. Pannetier, *J. Catal.* , 1972, **24**, 434-445.
45. D. Y. Kim, N. Singh, H. M. Lee and K. S. Kim, *Chem.-Eur. J.*, 2009, **15**, 5598-5604.
46. W. R. Nutt and M. L. McKee, *Inorg. Chem.* , 2007, **46**, 7633-7645.
47. T. B. Lee and M. L. McKee, *Inorg. Chem.* , 2009, **48**, 7564-7575.
48. D. Y. Kim, H. M. Lee, J. Seo, S. K. Shin and K. S. Kim, *Phys. Chem. Chem. Phys.* , 2010, **12**, 5446-5453.
49. C. Wu, G. Wu, Z. Xiong, X. Han, H. Chu, T. He and P. Chen, *Chem. Mater.* , 2010, **22**, 3-5.
50. R. Moury, U. B. Demirci, V. Ban, Y. Filinchuk, T. Ichikawa, L. Zeng, K. Goshome and P. Miele, *Chem. Mater.* , 2014, **26**, 3249-3255.
51. Z. Tang, H. Chen, X. Chen, L. Wu and X. Yu, *J. Am. Chem. Soc.* , 2012, **134**, 5464-5467.